AGU ADVANCING EARTH AND SPACE SCIENCE

Geophysical Research Letters®

RESEARCH LETTER
10.1029/2021GL096804

A Multivariate Flash Drought Indicator for Identifying Global Hotspots and Associated Climate Controls

Sourav Mukherjee[1] and Ashok Kumar Mishra[1]

[1]Glenn Department of Civil Engineering, Clemson University, Clemson, SC, USA

Key Points:

- A multivariate flash drought indicator is proposed to identify key hotspots locations across the globe
- Meteorological forcings show a varying and cascading effect on regional flash drought evolution
- Multivariate indicator identifies humid regions as most vulnerable to flash drought with exceptional intensification rates

Supporting Information:

Supporting Information may be found in the online version of this article.

Correspondence to:

A. K. Mishra,
ashokm@g.clemson.edu

Citation:

Mukherjee, S., & Mishra, A. K. (2022). A multivariate flash drought indicator for identifying global hotspots and associated climate controls. *Geophysical Research Letters*, *49*, e2021GL096804. https://doi.org/10.1029/2021GL096804

Received 29 OCT 2021
Accepted 26 DEC 2021

Author Contributions:

Conceptualization: Sourav Mukherjee, Ashok Kumar Mishra
Formal analysis: Sourav Mukherjee
Funding acquisition: Ashok Kumar Mishra
Investigation: Sourav Mukherjee
Methodology: Sourav Mukherjee, Ashok Kumar Mishra
Supervision: Ashok Kumar Mishra
Validation: Sourav Mukherjee
Writing – original draft: Sourav Mukherjee
Writing – review & editing: Ashok Kumar Mishra

Abstract The significant impact of flash droughts (FDs) on society can vary based on a combination of FD characteristics (event counts, mean severity, and rate of intensification), which is largely unexplored. We employed root-zone soil-moisture for 1980–2018 to calculate the FD characteristics and integrated them to formulate a novel multivariate FD indicator for mapping the global FD hotspot regions. The potential influence of climate characteristics (i.e., anomalies, aridity, and evaporative fractions) and land-climate feedbacks on the evolution of multivariate FD indicator is investigated. Our results indicate that precipitation is the primary driver of FD evolution, while the effect of temperature, vapor pressure deficit, and land-climate interaction varies across the climate divisions after the onset of the events. The magnitude of multivariate FD indicator decreases with increased climate aridity, and it is significant in the global humid regimes, underscoring the importance of water and energy supply as limiting factors regulating FD-risk.

Plain Language Summary Flash drought (FD) can significantly impact multiple sectors (e.g., agriculture, economy, and environment) very rapidly. Previous studies focused on a subset of FD characteristics at a time and over confined locations. In the light of such diversification, this study, for the first time, explored the most dominant climate controls of global FDs using an integrated approach that combines the FD frequency, severity, and intensification rates into a composite indicator. The results highlight the critical FD hotspots for prioritization and intervention. The key findings strengthen our perspective on FDs by improving our knowledge of the underlying physical processes and essential drivers across different climate divisions and ecosystems. The findings can be further extended to explore the combined influence of seasonality and magnitude of climate variables and develop suitable mitigation strategies to minimize the impact of FD events.

1. Introduction

Drought is a creeping phenomenon that slowly evolves over time and gradually spreads over large geographical areas resulting in significant environmental and socio-economic impacts (Mishra & Singh, 2010; Mukherjee et al., 2018; Wilhite, 1993). However, a substantial number of drought events are characterized by rapid intensification over a short period, sustaining over a few days to weeks. This rapid intensification is triggered by a complex interaction between sharply elevated atmospheric demand, limited soil moisture, and abruptly higher than usual temperatures, a phenomenon termed "flash drought" (FD) (Christian et al., 2020; Mo & Lettenmaier, 2016; Otkin et al., 2018; Svoboda et al., 2002). FD events are generally unforeseen and difficult to predict, which is why they end up causing devastating socio-economic impacts (Ford & Labosier, 2017; Jin et al., 2019; Mallya et al., 2013; Otkin et al., 2016). The coevolution of highly anomalous meteorological (e.g., precipitation and temperature) conditions relative to the climatological mean and the background state (e.g., aridity) of the region serve as key precursors for the onset and propagation of FDs (Apurv & Cai, 2020; Mo & Lettenmaier, 2015; Otkin et al., 2018; Pendergrass et al., 2020; L. Wang et al., 2016). Besides, the abrupt transition from an energy-limited to a water-stressed state (Seneviratne et al., 2010) can create favorable conditions for the onset of these events.

Many regional studies have reported increased FD occurrences and intensification across the humid, sub-humid, and semi-arid evaporation regimes of significant regions, such as China and the United States (Anderson et al., 2016; Christian et al., 2019; Mo & Lettenmaier, 2016; Nguyen et al., 2019; Otkin et al., 2016; Yuan et al., 2018). Recent FD-related studies have also investigated how the onset and propagation of these events are associated with natural climate variability (Mahto & Mishra, 2020; L. Wang et al., 2016) or anthropogenic warming (Yuan, Zheng, et al., 2019). The FD events can be different based on their characteristics (e.g., frequency, severity, and rate of intensification), and as a result a composite metric can better characterize FDs. Previous studies mostly used a single FD characteristic which may underestimate the FD impact assessments and identification of

vulnerable regions (Anderson et al., 2016; Christian et al., 2019; Ford & Labosier, 2017; Mahto & Mishra, 2020; Otkin et al., 2016, 2018). Furthermore, land-atmosphere interaction plays an important role in the occurrence and modulation of droughts (Berg & Sheffield, 2018); however, its role in the evolution of FD remains unexplored. Such interactions are often evaluated based on the covariance of soil moisture with surface temperature via the surface turbulent energy fluxes, known as soil-moisture temperature coupling strength, helpful for explaining drought intensification in the context of the coupled soil-atmosphere system (Berg et al., 2014; Berg & Sheffield, 2018; Hirsch et al., 2014; Miralles et al., 2012; Seneviratne et al., 2010). This provides a unique opportunity to assimilate the sub-indicators of FD characteristics into a composite metric for identifying the hotspots of FDs, and subsequently investigate the development of FDs in response to the regional climate controls and land-climate interactions, neither of which is explicitly nor sufficiently reported in the literature.

The primary goal of this study is to develop a novel multivariate FD indicator, and subsequently identify global hotspots and to investigate further the potential role of climate and surface energy partitioning on the evolution of FD events. Specifically, we aim to answer the following questions: (a) what are the FD hotspots based on a multivariate FD indicator (MFDI) that combines the essential characteristics (or variables) of FD events (e.g., frequency, severity, and rate of intensification)? (b) how does the regional hydroclimatic forcing impact the evolution of FDs for the hotspot locations and across the 26 IPCC-AR5 climate divisions? And (c) what is the effect of surface energy partitioning on the FDs as well as on the MFDI? The rest of the paper is structured as follows. Section 2 describes the data and methodology applied in the study. Section 3 provides results and discussion, followed by a conclusion in Section 4.

2. Methods

2.1. Data

Root-zone soil moisture (RZSM) was derived from hourly data obtained for the three soil-layers (layer 1: 0–7 cm, layer 2: 7–28 cm, layer 3: 28–100 cm) from the European Center for Medium-Range Weather Forecasts Reanalysis 5 (ERA5) for the period, 1980–2018. Other daily variables, such as total precipitation (Pr), minimum and maximum temperature (T_{min}, and T_{max}), surface pressure (P_{surf}), actual evaporation (Ev), and potential evaporation (Ep), are similarly derived from ERA5. These climate variables, along with vapor pressure deficit (VPD) and soil-moisture temperature coupling (denoted as pi), are converted to their pentad (5-day) mean and used to investigate the regional effect of hydroclimate variable on FDs globally and across the hotspot climate divisions. A brief discussion on the calculation of VPD and pi is provided in Text S1 and S2 in the Supporting Information S1.

2.2. Flash Drought Identification Methodology

FD events are identified based on pentad (5-day) mean RZSM using the methodology proposed by Yuan, Zheng, et al. (2019). The methodology combines the criteria of rapid decline in RZSM and dry persistency. In this method, the detection of FD is employed based on the following three criteria (Yuan, Zheng, et al., 2019):

1. The pentad mean RZSM decreases from above 40th percentile to below 20th percentile, with an average decline rate of no less than 5% in RZSM percentiles for each pentad.
2. The FD is considered to have terminated if the declined RZSM rises to 20th percentile again. These two criteria determine the onset and termination stages of an FD event.
3. The drought should last for at least 3 pentads (15 days).

The first two criteria describe the onset and termination of an FD event. The 40th percentile indicates no drought conditions and is consistent with the drought classification system suggested by the United States Drought Monitor (USDM). The use of 20th percentile excludes events that last longer than 3–6 months, which should be regarded as seasonal droughts instead of FDs. The third criterion is the minimal duration of the FD episodes, which eliminates those events that last no longer than 10 days, therefore, likely to have almost no potential impact.

2.3. Calculation of FD Severity and Intensification

The FD identification methodology (Yuan, Zheng, et al., 2019) implemented in this study can capture rapid changes in drying, which directly relates to vegetation health and high sensitivity toward the termination of

drought events from rain. However, the existing methodology does not provide a direct metric for calculating the FD intensity and severity. Therefore, we extend the existing methodology to calculate FD severity and rate of intensification (referring to the speed or flashiness) as explained below:

1. *FD severity*
   The severity of FD events is calculated as the difference in RZSM percentiles between the initiation and termination pentads of FD events (see Figure S1 in Supporting Information S1 for illustration).
2. *FD intensification rate*
   The rate of intensification is calculated as the average rate of depletion (RD) of RZSM (in percentiles) considering all pentad-to-pentad changes (%) starting from the initiation until the termination of the FD events (see Figure S1 for illustration) given as,

$$RD = \frac{\sum_{i=1}^{d} rd_i}{d} \tag{1}$$

   where, $rd_i = \left(\frac{RZSM_{i-1} - RZSM_i}{RZSM_{i-1}}\right) \times 100$, d = duration of FD event expressed as the number of pentads, and $RZSM_i$ denote the RZSM percentile at the ith pentad. The FD events are thus classified into mild (RD < 20% per pentad), severe (20% ≤ RD < 30% per pentad), extreme (30% ≤ RD < 40% per pentad), and exceptional (RD ≥ 40% per pentad) events based on the magnitude of RD. This classification is similar to the one applied by Christian et al. (2019).

2.4. Calculation of Multivariate Flash Drought Indicator

The socio-economic impact of drought can vary based on its multivariate characteristics such as drought frequency, severity, and intensity (Rajsekhar et al., 2015). Thus, a comprehensive approach is recommended to combine these multivariate characteristics in a unique metric to assess the potential impact of FDs. In this study, we used the Mazziotta-Pareto Index (MPI; De Muro et al., 2011) method to calculate a multivariate FD indicator (MFDI). MPI is a non-linear composite index method that transforms a set of individual indicators considered "non-substitutable," meaning all components must be "balanced" in standardized variables. Here, the MFDI represents the magnitude by which a region is affected by FDs, whose dimensions are built by integrating normalized dimensions of three FD characteristics: (a) total FD event counts, (b) mean severity, and (c) average rate of intensification across the global grid-locations. The magnitude of MFDI increases with the individual increases in any of the subset characteristics, suggesting a positive association with the vulnerability of a region to FDs. The main advantage of MFDI is that it integrates three FD characteristics valuable for regional FD analysis, which is more informative compared with individual metric-based analysis.

The MPI methodology first employs normalization of variables (referring to the normalized dimensions of FD characteristics) which are finally integrated using an arithmetic mean adjusted by a *penalty* coefficient related to the variability of each unit. Here, units refer to the grid locations across the global land area. Particularly, this method applies the coefficient of variation as a penalty and has been useful for formulating robust composite indicators for various real-world applications (Greco et al., 2019; Mazziotta & Pareto, 2016). The calculation of MFDI using the MPI method (De Muro et al., 2011) can be formalized in two steps as explained below:

1. Normalization
   Let $X = \{x_{ij}\}$ be the matrix with n rows (representing the number of global 0.5° × 0.5° grid-locations or units) and m columns (here representing subsets of FD characteristics, e.g., total FD counts, mean severity, and mean RD) and, the standardized matrix, $Z = \{Z_{ij}\}$ is then given as,

$$z_{ij} = 100 \pm \frac{(x_{ij} - M_{x_j})}{S_{x_j}} 10 \tag{2}$$

   where Z is transformed using a common scale with mean = 100 and standardized deviation = 10, M_{xj} and S_{xj} denote the mean and the standard deviation of the jth indicator given as,

$$M_{x_j} = \frac{\sum_{i=1}^{n} x_{ij}}{n};\quad S_{x_j} = \sqrt{\frac{\sum_{i=1}^{n} (x_{ij} - M_{x_j})^2}{n}}.$$

The sign ± depends on the relation of the *j*th indicator with the MFDI. In this study, we used a positive sign following the positive association between FD counts, severity, and intensification rate with the MFDI.

2. Aggregation

Let cv_i be the coefficient of variation for the *i*th unit:

$$cv_i = \frac{S_{z_i}}{M_{z_i}} \tag{3}$$

where $M_{z_i} = \frac{\sum_{j=1}^{m} z_{ij}}{m};\quad S_{z_i} = \sqrt{\frac{\sum_{j=1}^{m} (z_{ij} - M_{z_i})^2}{m}}$

Then, the generalized form of MPI is given by:

$$MPI_i^{+/-} = M_{z_i}(1 \pm cv_i^2) = M_{z_i} \pm S_{z_i} cv_i \tag{4}$$

where the sign of the penalty (the product $S_{z_i} cv_i$) depends on the kind of phenomenon to be measured and the association of individual indicators with the phenomenon. In this study, the indicators are ''increasing'' or ''positive'', that is, increasing values of the indicator (or FD characteristics) correspond to positive variations of the MFDI or the potential effect of FDs. Therefore, we used MPI^- to calculate the values of MFDI. It is important to note that the drought indices can be derived in different ways, and these indices can be compared by standardizing the time series. There are different concepts available for standardizing composite indicators, including aggregation and weighting schemes (Greco et al., 2019; Mazziotta & Pareto, 2016; Mukherjee et al., 2021). In this study, we use a common scale with mean = 100 and standardized deviation = 10, as indicated by Equation 2, such that the values of MFDI fall approximately in the range (70; 130). Subsequently, an MFDI value exceeding 100 (the standardizing mean) is used to indicate the hotspot location of FDs across the globe. In other words, the hotspots of FDs are identified based on the locations where the MFDI values exceed the standardizing mean of 100.

3. Results and Discussion

3.1. Global Hotspots of Flash Drought

We investigated global hotspots of FD based on the magnitude of MFDI across the global grid-locations (or units; see Section 2) considering the 1980–2018 period. As such, a higher magnitude of MFDI over a given location in a climate division indicates that FD events are relatively more frequent, severe, and flashy in the region, and thus can be considered as one of the hotspot locations of FD. Figure 1 illustrates the spatial distribution of MFDI for the globe and across the 26 IPCC-AR5 climate divisions. Due to the normalization scheme employed in this study (as demonstrated by Equation 2 in Section 2), a particular location with MFDI magnitude greater than 100 is considered as a hotspot.

Based on the magnitude of MFDI (Figure 1a), hotspots of FDs are apparent in many parts of Central and Eastern North America (CAN and ENA), Amazon (AMZ) basin and Southern and Western South America (SSA and WSA), Southern, Southeastern, and Eastern Asia (SAS, SEA, and EAS), and Central and Northern Europe (CEU and NEU). Majority of these climate divisions show MFDI magnitude greater than 100. These 10 climate divisions show relatively higher magnitude of mean MFDI greater than 100 as illustrated by the boxplots in Figure 1b, with Eastern North America noted as the most affected climate division.

The hotspots illustrated in the spatial map of Figure 1a closely match with the spatial distribution of relatively higher FD count, mean severity, and RD as noted in Figure S2 in Supporting Information S1. This is also suggested by the shaded 3D-scatter plot in Figure 1b that illustrates the positive association between the individual FD characteristics and the MFDI based on the global grid locations. More importantly, the hotspot locations are in close agreement with regional spatial pattern of higher FD frequency reported in previous studies, such as across the humid regions of Eastern North America (Ford & Labosier, 2017), and Eastern China (Yuan, Zheng, et al., 2019).

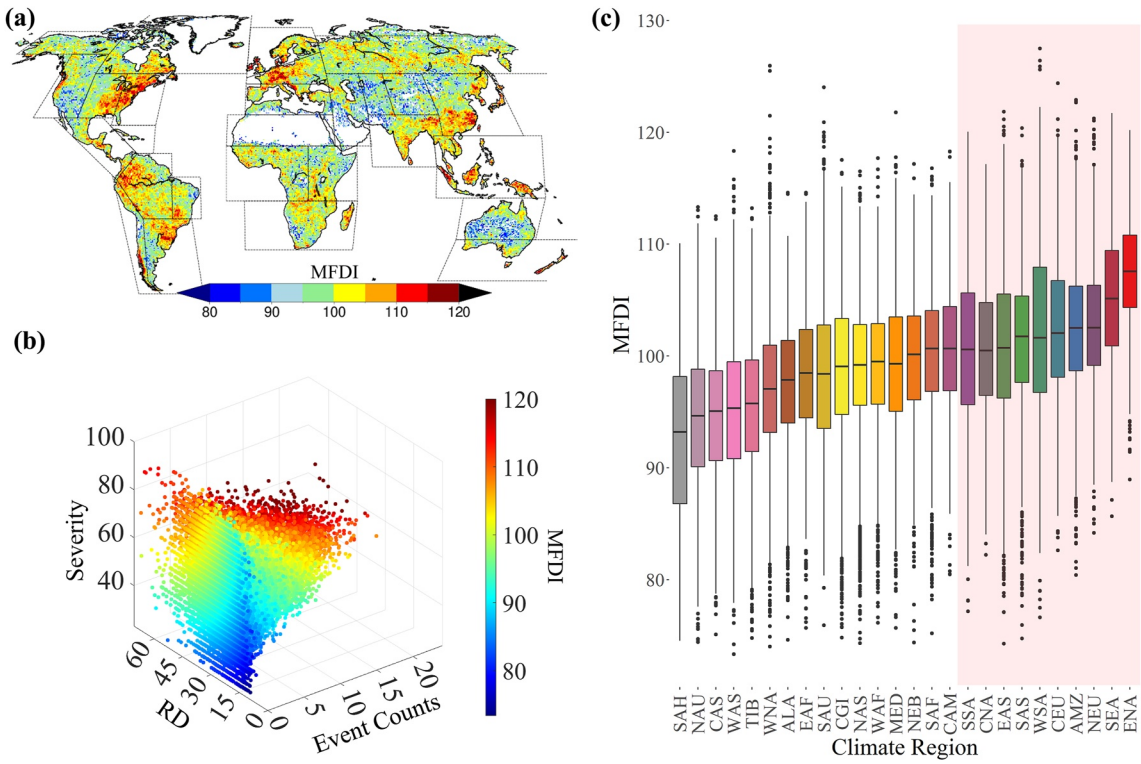

Figure 1. (a) Spatial map showing the hotspot locations based on the MFDI evaluated for the global grid-locations for the period, 1980–2018, (b) 3D scatter plot showing the association between the total FD event counts, mean severity, rate of depletion (RD) of RZSM and MFDI for the global grid-locations, and (c) boxplots showing the spatial distribution of MFDI across the 26 IPCC-AR5 climate divisions, arranged in ascending order (from left to right) of the mean MFDI magnitude.

3.2. Effect of Regional Climate on Flash Drought Evolution

Droughts are primarily triggered by climatic perturbations such as abnormal precipitation and temperature variations (Hanel et al., 2018; Ionita et al., 2017; Konapala et al., 2020), an abrupt rise in atmospheric evaporative demand (Vicente-Serrano et al., 2020), and positive land-atmospheric feedback loops (Gevaert et al., 2018; Kumar et al., 2020; Miralles et al., 2012). These climate fluctuations are a sub-set of anticyclonic conditions that inhibit low-level moisture convergences (Mukherjee et al., 2020) at different spatial and temporal scales. More importantly, these climate anomalies often have a cascading effect on the rapid intensification of evaporative stress and soil moisture depletion leading to more favorable conditions for the onset and propagation of FDs.

We adopted a holistic approach to investigate the climate versus FD dynamics in the context of the evolution of FD events for the 26 climate divisions. We selected pentad mean of daily total precipitation (Pr), maximum 2m air temperature (T_{max}), VPD, and soil-temperature coupling strength (pi; Miralles et al., 2012; Seneviratne et al., 2010) for total nine pentads, five pentads before, during, and three pentads after the initiation of FD event. The standardized anomalies of each of these variables are then derived with respect to their climatological pentad mean (for the 1980–2018 period). Figures S3–S6 in Supporting Information S1 illustrate the spatiotemporal distribution of the mean standardized anomalies corresponding to the selected pentads. The temporal variation of the distribution of these anomalies is further demonstrated as boxplots for the 26 climate divisions in Figure 2 and Figure S7 in Supporting Information S1 for the selected four pentads, starting from the initiation of the events (denoted by pentad number zero). To preserve all information related to the regional climate effects, the boxplots are derived based on all events and every grid location located within a given climate division.

The results suggest a cascading effect of key regional hydroclimatic forcings on FDs (Figure 2 and Figures S3–S7 in Supporting Information S1). The spatial maps suggest that no significant anomalies of the selected variables (Pr, T_{max}, VPD, and pi) are noted during pentad −5 to −1 before the onset of the FD events (Figures S3–S6 in

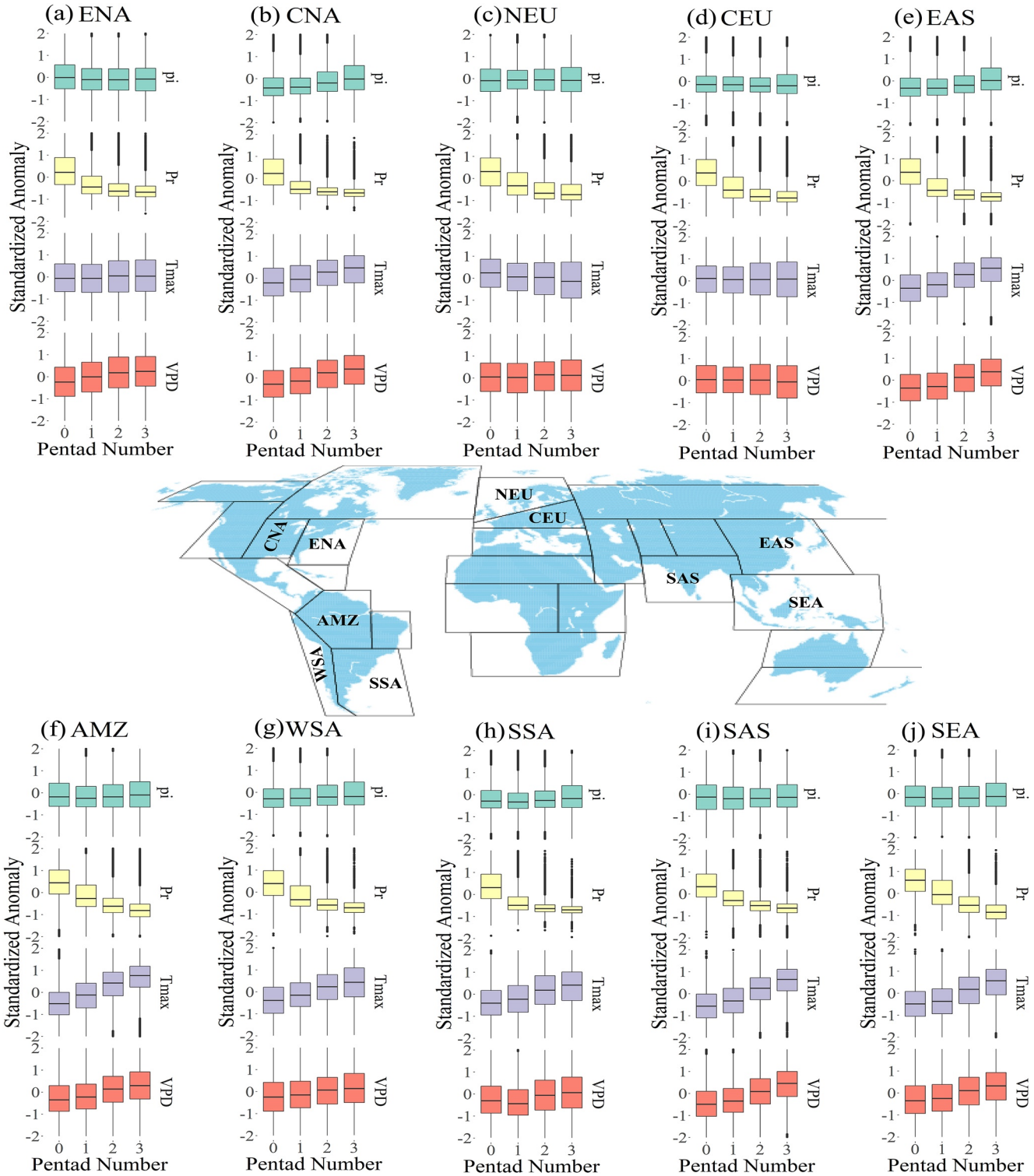

Figure 2. Effect of hydro-meteorological forcing, pi, Pr, T_{max}, and VPD on FD evolution for top 10 most affected climate divisions.

Supporting Information S1). On the other hand, the significant positive (T_{max}, VPD, and pi) and negative (Pr) anomalies usually appear during the evolution of the FD events, that is, after the onset of the events (at pentad number zero). The boxplots in Figure 2 and Figure S7 in Supporting Information S1 further reinforce these findings on the regional scale.

The values of Pr anomalies progressively and rapidly decrease as the event progresses after the initiation of the drought for all climate divisions. Pr exhibit the most dominant effect on the depletion of RZSM during the FD evolution across all climate divisions. Interestingly, the positive effect of Tmax is significantly substantial in all climate divisions, except for Eastern North America (ENA), and Northern and Central Europe (NEU and CEU), CGI, and ALA. Similarly, Northern and Central Europe (NEU and CEU), ALA, and CGI exhibit no effect of VPD on FDs, while a significant positive effect of VPD is notable in all other climate divisions. FD evolution is found to be significantly associated with pi in Central North America (CAN), East Asia (EAS), and other climate divisions such as CAM, NAU, NAS, TIB, WAS, WNA, ALA, and CGI. Relatively stronger positive effect of soil moisture-temperature coupling in one of the hotspots, Central North America, can be linked explicitly to the more extended soil-moisture memory and general drought characteristics in the Great Plains regions (Livneh & Hoerling, 2016). Overall, our results are in close agreement with regional studies specific to FD that suggest a similar spatio-temporal pattern of climatic forcings specific to FD onset and evolution (Christian et al., 2020; Ford & Labosier, 2017).

3.3. Effect of Surface Energy Partitioning

Climate anomalies and surface energy fluxes significantly control the hydrological cycle and global water availability (Beltrami & Kellman, 2003; Entekhabi et al., 1996; Forzieri et al., 2020; Hao et al., 2018; Ionita et al., 2017; Konapala et al., 2020). The complex mechanism responsible for the intensification of drought is potentially dependent on the background aridity and type of evaporation (energy or water-limited) regime (Forzieri et al., 2020; Mukherjee & Mishra, 2021; Su et al., 2021). Specifically, different evaporation regimes have distinct surface energy partitioning, governed by climate aridity, that affects soil evaporation in the energy-limited and water-limited regimes with varying complexity (Berg et al., 2014). Therefore, the type of evaporation regime can significantly control the FD frequency, severity and rate of intensification individually, and MFDI, that integrates all these information.

We investigate the potential influence of climate aridity and evaporative fraction on the occurrence of FD events. Climate aridity is evaluated based on the aridity index (AI), calculated as a ratio of the mean annual Ep to Pr (see Text S3 in the Supporting Information S1). Based on the AI, the global land areas are then divided into humid, sub-humid, and semi-arid regions (UNEP & Thomas, 1992). In this study, the semi-arid and sub-humid regimes are classified as transitional regimes, indicating the regions that fall within the arid ($AI > 5$) and humid ($AI < 1.5$) evaporation regimes. The humid and transitional (sub-humid and semi-arid) evaporation regimes are presented in Figure 3a. Evaporative fraction is calculated as a ratio of mean annual Ev to Pr, and dashed lines in Figure 3b represent the energy and water limits. In addition, the potential effect of humid and transitional evaporation regimes on the variation of MFDI is also examined (see bold black line in Figure 3b). The gridded MFDI values are averaged across the grid-locations falling within incremental bins of 0.25 intervals of climate aridity (ranging from 0 to 5). Investigating such variation of MFDI is expected to associate the potential role of climate aridity on the integrated FD characteristics (frequency, severity, and rate of intensification). Only FD events that exhibit an exceptionally high rate of intensification ($RD \geq 40\%$ per pentad; see Section 2), capable of causing significant socio-economic losses, are considered in the analysis.

The shaded scatterplots indicate that a significant number of events occurred in the grid-locations encompassed within the humid evaporation regimes (energy-limited with climate aridity <1.5) as compared to the transitional evaporation regimes ($1.5 \leq$ climate aridity < 5). Even the number of FD events decreases within the transitional regime with a shift from sub-humid to semi-arid regimes between climate aridity values 1.5–5. However, evaporative fractions do not show any dominant effect on the FD occurrences. A similar variation is noted for the MFDI that shows a peak value of 106.5 for humid regimes and exhibits a steady decrease up to less than 100 as the climate aridity decreases continuously from the humid to the transitional (semi-arid) regimes. These results indicate that the FD events, characterized by the exceptional depletion rate of RZSM, are more frequent in the humid-ecosystems, and their potential effect, defined by the MFDI magnitude, is substantially higher in those regions.

Overall, such associations can be driven by the difference in initial RZSM conditions and more extended memory of soil moisture in wetter regimes (Hagemann & Stacke, 2015; Liang & Yuan, 2021; Seneviratne et al., 2006). For example, energy-limited and water-limited regimes have different transferability rates of soil temperature memory that govern the atmospheric persistence, which significantly affects drying rates (Gerken et al., 2019). In

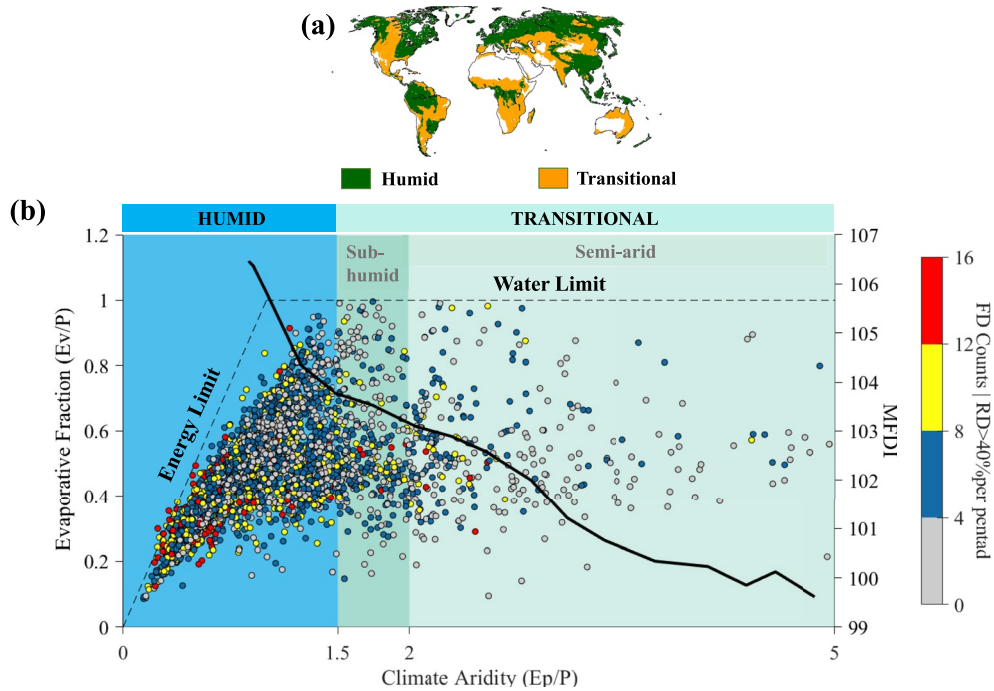

Figure 3. (a) Spatial map showing the global humid and transitional regimes for the globe based on values of climate aridity, and (b) effect of surface energy partitioning -- shown by scatterplots of event counts with average rate of depletion (RD) of RZSM of at least 40% per pentad (exceptional intensification rate) corresponding to the grid-locations with given climate aridity (shown in *x*-axis), and evaporative fraction (left *y*-axis). The solid black line indicates the MFDI values (shown in right *y*-axis) averaged across the grid-locations falling within incremental bins (at intervals of 0.25) of climate aridity ranging from 0 to 5 (as shown in the *x*-axis).

addition, variations in climate controls can also be linked to the difference in the variation of ecosystem functions, such as water-use efficiency, that are primarily governed by surface energy partitioning between water-limited and energy-limited regimes (Roderick & Farquhar, 2011; Yang et al., 2016).

4. Conclusion

A comprehensive analysis of FDs is performed in this study to identify the hotspot locations and enhance the scientific understanding of the climate versus FD dynamics globally and across the 26 IPCC-AR5 climate divisions for the period 1980–2018. We developed a novel multivariate flash drought indicator (MFDI) by integrating three FD characteristics (total FD counts, mean severity, and average rate of intensification) for the global grid locations. The MFDI is utilized to generate a global map for the hotspot location and the most affected IPCC AR-5 climate divisions.

The results from the study suggest potential hotspot locations across majority of Central and Eastern North America, Amazon basin and Southern and Western South America, Southern, Southeastern, and Eastern Asia, and Central and Northern Europe. Our analyses provide evidence that climate variables, such as precipitation, temperature, VPD, and soil-moisture temperature coupling, have a varying and cascading (or sequential) impact on regional FD evolution. While precipitation plays the most dominant role in all climate divisions, Tmax and VPD are prominent across most hotspot locations except for Central and Northern Europe. On the other hand, a considerable effect of soil moisture-temperature coupling strength (pi) is only noted in Central North America and East Asia. The surface-energy partitioning revealed dominant control of climate aridity on the occurrence of exceptionally intense FD events. We found that FD events with exceptional intensification rates (i.e., average rate of pentad-to-pentad RZSM depletion $\geq$ 40%) are more frequent in the humid regimes than the sub-humid and semi-arid regimes. These higher intensification rates are primarily driven by the difference in initial RZSM conditions and more extended memory of soil moisture in wetter regimes (Hagemann & Stacke, 2015; Liang & Yuan, 2021; Seneviratne et al., 2006).

Overall, identifying global-scale FD hotspots will provide valuable information to policymakers, experts, and stakeholders dealing with agriculture sectors and ecosystems services in different parts of the world. Leveraging the hotspot-specific information to identify the critical regional and climatological drivers reveals which precursors should be given more weightage for developing forecasting tools to minimize the impact of FDs on different socio-economic sectors. The new information gained in this study can be further extended to formalize multi-hazard risk assessment and prevailing vulnerabilities of exposed ecosystems. Some limitations of the study include the simplicity of the MPI methodology. Although it is fairly adjusted to account for the imbalance among the indicators with its "penalty" component (Greco et al., 2019; Mazziotta & Pareto, 2016), more attention is needed on the aggregation of FD characteristics. The scientific understanding of the underlying FD mechanisms can be further explored by exploring causal linkages between soil moisture memory length, vegetation fluxes, and water use efficiency of crops, and the coupled changes in magnitude and seasonality of climate variables that can alter the spatiotemporal distribution of FD characteristics at a global scale. More research is needed for developing suitable (sub-seasonal) FD forecasting tools and early warnings (Pendergrass et al., 2020) across the FD hotspots.

Data Availability Statement

The authors are thankful for the data provided by the European Centre for Medium-Range Weather Forecasts Reanalysis 5 (https://cds.climate.copernicus.eu/cdsapp#!/dataset/reanalysis-era5-single-levels?tab=form).

Acknowledgments
This study was supported by the National Science Foundation (NSF) awards # 1653841 and 1841629. Additionally, the authors thank editor, Dr. Valeriy Ivanov, and the reviewers for their valuable and constructive feedback to improve the original manuscript.

References

Anderson, M. C., Zolin, C. A., Sentelhas, P. C., Hain, C. R., Semmens, K., Tugrul Yilmaz, M., et al. (2016). The Evaporative Stress Index as an indicator of agricultural drought in Brazil: An assessment based on crop yield impacts. *Remote Sensing of Environment*, *174*, 82–99. https://doi.org/10.1016/j.rse.2015.11.034

Apurv, T., & Cai, X. (2020). Drought propagation in contiguous US watersheds: A process-based understanding of the role of climate and watershed properties. *Water Resources Research*, *56*(9), e2020WR027755. https://doi.org/10.1029/2020WR027755

Beltrami, H., & Kellman, L. (2003). An examination of short- and long-term air–ground temperature coupling. *Global and Planetary Change*, *38*(3), 291–303. https://doi.org/10.1016/S0921-8181(03)00112-7

Berg, A., Lintner, B. R., Findell, K. L., Malyshev, S., Loikith, P. C., & Gentine, P. (2014). Impact of soil moisture–atmosphere interactions on surface temperature distribution. *Journal of Climate*, *27*(21), 7976–7993. https://doi.org/10.1175/JCLI-D-13-00591.1

Berg, A., & Sheffield, J. (2018). Climate change and drought: The soil moisture perspective. *Current Climate Change Reports*, *4*(2), 180–191. https://doi.org/10.1007/s40641-018-0095-0

Christian, J. I., Basara, J. B., Hunt, E. D., Otkin, J. A., & Xiao, X. (2020). Flash drought development and cascading impacts associated with the 2010 Russian heatwave. *Environmental Research Letters*, *15*(9), 094078. https://doi.org/10.1088/1748-9326/ab9faf

Christian, J. I., Basara, J. B., Otkin, J. A., Hunt, E. D., Wakefield, R. A., Flanagan, P. X., & Xiao, X. (2019). A methodology for flash drought identification: Application of flash drought frequency across the United States. *Journal of Hydrometeorology*, *20*(5), 833–846. https://doi.org/10.1175/JHM-D-18-0198.1

De Muro, P., Mazziotta, M., & Pareto, A. (2011). Composite indices of development and poverty: An application to MDGs. *Social Indicators Research*, *104*(1), 1–18. https://doi.org/10.1007/s11205-010-9727-z

Entekhabi, D., Rodriguez-Iturbe, I., & Castelli, F. (1996). Mutual interaction of soil moisture state and atmospheric processes. *Journal of Hydrology*, *184*(1), 3–17. https://doi.org/10.1016/0022-1694(95)02965-6

Ford, T. W., & Labosier, C. F. (2017). Meteorological conditions associated with the onset of flash drought in the Eastern United States. *Agricultural and Forest Meteorology*, *247*, 414–423. https://doi.org/10.1016/j.agrformet.2017.08.031

Forzieri, G., Miralles, D. G., Ciais, P., Alkama, R., Ryu, Y., Duveiller, G., et al. (2020). Increased control of vegetation on global terrestrial energy fluxes. *Nature Climate Change*, *10*(4), 356–362. https://doi.org/10.1038/s41558-020-0717-0

Gerken, T., Ruddell, B. L., Yu, R., Stoy, P. C., & Drewry, D. T. (2019). Robust observations of land-to-atmosphere feedbacks using the information flows of FLUXNET. *Npj Climate and Atmospheric Science*, *2*(1), 1–10. https://doi.org/10.1038/s41612-019-0094-4

Gevaert, A. I., Miralles, D. G., de Jeu, R. A. M., Schellekens, J., & Dolman, A. J. (2018). Soil moisture-temperature coupling in a set of land surface models. *Journal of Geophysical Research: Atmospheres*, *123*(3), 1481–1498. https://doi.org/10.1002/2017JD027346

Greco, S., Ishizaka, A., Tasiou, M., & Torrisi, G. (2019). On the methodological framework of composite indices: A review of the issues of weighting, aggregation, and robustness. *Social Indicators Research*, *141*(1), 61–94. https://doi.org/10.1007/s11205-017-1832-9

Hagemann, S., & Stacke, T. (2015). Impact of the soil hydrology scheme on simulated soil moisture memory. *Climate Dynamics*, *44*(7), 1731–1750. https://doi.org/10.1007/s00382-014-2221-6

Hanel, M., Rakovec, O., Markonis, Y., Máca, P., Samaniego, L., Kyselý, J., & Kumar, R. (2018). Revisiting the recent European droughts from a long-term perspective. *Scientific Reports*, *8*(1), 9499. https://doi.org/10.1038/s41598-018-27464-4

Hao, Z., Singh, V. P., & Xia, Y. (2018). Seasonal drought prediction: Advances, challenges, and future prospects. *Reviews of Geophysics*, *56*.1, 108–141. Retrieved from https://agupubs.onlinelibrary.wiley.com/doi/full/10.1002/2016RG000549

Hirsch, A. L., Pitman, A. J., & Kala, J. (2014). The role of land cover change in modulating the soil moisture-temperature land-atmosphere coupling strength over Australia. *Geophysical Research Letters*, *41*(16), 5883–5890. https://doi.org/10.1002/2014GL061179

Ionita, M., Tallaksen, L., Kingston, D., Stagge, J., Laaha, G., Van Lanen, H., et al. (2017). The European 2015 drought from a climatological perspective. *Hydrology and Earth System Sciences*, *21*, 1397–1419. https://doi.org/10.5194/hess-21-1397-2017

Jin, C., Luo, X., Xiao, X., Dong, J., Li, X., Yang, J., & Zhao, D. (2019). The 2012 flash drought threatened US midwest agroecosystems. *Chinese Geographical Science*, *29*(5), 768–783. https://doi.org/10.1007/s11769-019-1066-7

Konapala, G., Mishra, A. K., Wada, Y., & Mann, M. E. (2020). Climate change will affect global water availability through compounding changes in seasonal precipitation and evaporation. *Nature Communications*, *11*(1), 3044. https://doi.org/10.1038/s41467-020-16757-w

Kumar, S., Newman, M., Lawrence, D. M., Lo, M.-H., Akula, S., Lan, C.-W., et al. (2020). The GLACE-hydrology experiment: Effects of land–atmosphere coupling on soil moisture variability and predictability. *Journal of Climate*, *33*(15), 6511–6529. https://doi.org/10.1175/JCLI-D-19-0598.1

Liang, M., & Yuan, X. (2021). Critical role of soil moisture memory in predicting the 2012 Central United States flash drought. *Frontiers of Earth Science*, *9*. https://doi.org/10.3389/feart.2021.615969

Livneh, B., & Hoerling, M. P. (2016). The physics of drought in the U.S. Central Great Plains. *Journal of Climate*, *29*(18), 6783–6804. https://doi.org/10.1175/JCLI-D-15-0697.1

Mahto, S. S., & Mishra, V. (2020). Dominance of summer monsoon flash droughts in India. *Environmental Research Letters*, *15*, 104061. https://doi.org/10.1088/1748-9326/abaf1d

Mallya, G., Zhao, L., Song, X. C., Niyogi, D., & Govindaraju, R. S. (2013). 2012 Midwest drought in the United States. *Journal of Hydrologic Engineering*, *18*(7), 737–745. https://doi.org/10.1061/(ASCE)HE.1943-5584.0000786

Mazziotta, M., & Pareto, A. (2016). On a generalized non-compensatory composite index for measuring socio-economic phenomena. *Social Indicators Research*, *127*(3), 983–1003. https://doi.org/10.1007/s11205-015-0998-2

Miralles, D. G., van den Berg, M. J., Teuling, A. J., & de Jeu, R. A. M. (2012). Soil moisture-temperature coupling: A multiscale observational analysis. *Geophysical Research Letters*, *39*(21). https://doi.org/10.1029/2012GL053703

Mishra, A. K., & Singh, V. P. (2010). A review of drought concepts. *Journal of Hydrology*, *391*(1), 202–216. https://doi.org/10.1016/j.jhydrol.2010.07.012

Mo, K. C., & Lettenmaier, D. P. (2015). Heat wave flash droughts in decline. *Geophysical Research Letters*, *42*(8), 2823–2829. https://doi.org/10.1002/2015GL064018

Mo, K. C., & Lettenmaier, D. P. (2016). Precipitation deficit flash droughts over the United States. *Journal of Hydrometeorology*, *17*(4), 1169–1184. https://doi.org/10.1175/JHM-D-15-0158.1

Mukherjee, S., Ashfaq, M., & Mishra, A. K. (2020). Compound drought and heatwaves at a global scale: The role of natural climate variability-associated synoptic patterns and land-surface energy budget anomalies. *Journal of Geophysical Research: Atmospheres*, *125*(11), e2019JD031943. https://doi.org/10.1029/2019JD031943

Mukherjee, S., Mishra, A., & Trenberth, K. E. (2018). Climate change and drought: A perspective on drought indices. *Current Climate Change Reports*, *4*(2), 145–163. https://doi.org/10.1007/s40641-018-0098-x

Mukherjee, S., & Mishra, A. K. (2021). Increase in compound drought and heatwaves in a warming world. *Geophysical Research Letters*, *48*(1), e2020GL090617. https://doi.org/10.1029/2020GL090617

Mukherjee, S., Mishra, A. K., Mann, M. E., & Raymond, C. (2021). Anthropogenic warming and population growth may double US heat stress by the late 21st century. *Earth's Future*, *9*(5), e2020EF001886. https://doi.org/10.1029/2020EF001886

Nguyen, H., Wheeler, M. C., Otkin, J. A., Cowan, T., Frost, A., & Stone, R. (2019). Using the evaporative stress index to monitor flash drought in Australia. *Environmental Research Letters*, *14*(6), 064016. https://doi.org/10.1088/1748-9326/ab2103

Otkin, J. A., Anderson, M. C., Hain, C., Svoboda, M., Johnson, D., Mueller, R., et al. (2016). Assessing the evolution of soil moisture and vegetation conditions during the 2012 United States flash drought. *Agricultural and Forest Meteorology*, *218–219*, 230–242. https://doi.org/10.1016/j.agrformet.2015.12.065

Otkin, J. A., Svoboda, M., Hunt, E. D., Ford, T. W., Anderson, M. C., Hain, C., & Basara, J. B. (2018). Flash droughts: A review and assessment of the challenges imposed by rapid-onset droughts in the United States. *Bulletin of the American Meteorological Society*, *99*(5), 911–919. https://doi.org/10.1175/BAMS-D-17-0149.1

Pendergrass, A. G., Meehl, G. A., Pulwarty, R., Hobbins, M., Hoell, A., AghaKouchak, A., et al. (2020). Flash droughts present a new challenge for subseasonal-to-seasonal prediction. *Nature Climate Change*, *10*(3), 191–199. https://doi.org/10.1038/s41558-020-0709-0

Rajsekhar, D., Singh, V P., & Mishra, A K. (2015). Multivariate drought index: An information theory based approach for integrated drought assessment. *Journal of Hydrology*, *526*, 164–182. https://doi.org/10.1016/j.jhydrol.2014.11.031

Roderick, M. L., & Farquhar, G. D. (2011). A simple framework for relating variations in runoff to variations in climatic conditions and catchment properties. *Water Resources Research*, *47*(12). https://doi.org/10.1029/2010wr009826

Seneviratne, S. I., Corti, T., Davin, E. L., Hirschi, M., Jaeger, E. B., Lehner, I., et al. (2010). Investigating soil moisture–climate interactions in a changing climate: A review. *Earth-Science Reviews*, *99*(3), 125–161. https://doi.org/10.1016/j.earscirev.2010.02.004

Seneviratne, S. I., Koster, R. D., Guo, Z., Dirmeyer, P. A., Kowalczyk, E., Lawrence, D., et al. (2006). Soil moisture memory in AGCM simulations: Analysis of global land–atmosphere coupling experiment (GLACE) data. *Journal of Hydrometeorology*, *7*(5), 1090–1112. https://doi.org/10.1175/JHM533.1

Su, J., Gou, X., HilleRisLambers, J., Deng, Y., Fan, H., Zheng, W., et al. (2021). Increasing climate sensitivity of subtropical conifers along an aridity gradient. *Forest Ecology and Management*, *482*, 118841. https://doi.org/10.1016/j.foreco.2020.118841

Svoboda, M., LeComte, D., Hayes, M., Heim, R., Gleason, K., Angel, J., et al. (2002). The drought monitor. *Bulletin of the American Meteorological Society*, *83*(8), 1181–1190. https://doi.org/10.1175/1520-0477-83.8.1181

UNEP & Thomas, D. (1992). *World atlas of desertification* (pp. 15–45). Edward Arnold.

Vicente-Serrano, S. M., McVicar, T. R., Miralles, D. G., Yang, Y., & Tomas-Burguera, M. (2020). Unraveling the influence of atmospheric evaporative demand on drought and its response to climate change. *WIREs Climate Change*, *11*(2), e632. https://doi.org/10.1002/wcc.632

Wang, L., Yuan, X., Xie, Z., Wu, P., & Li, Y. (2016). Increasing flash droughts over China during the recent global warming hiatus. *Scientific Reports*, *6*(1), 30571. https://doi.org/10.1038/srep30571

Wilhite, D. A. (1993). The enigma of drought. In D. A. Wilhite (Ed.), *Drought assessment, management, and planning: Theory and case studies* (pp. 3–15). Boston, MA: Springer US. https://doi.org/10.1007/978-1-4615-3224-8_1

Yang, Y., Guan, H., Batelaan, O., McVicar, T. R., Long, D., Piao, S., et al. (2016). Contrasting responses of water use efficiency to drought across global terrestrial ecosystems. *Scientific Reports*, *6*(1), 23284. https://doi.org/10.1038/srep23284

Yuan, W., Zheng, Y., Piao, S., Ciais, P., Lombardozzi, D., Wang, Y., et al. (2019). Increased atmospheric vapor pressure deficit reduces global vegetation growth. *Science Advances*, *5*(8), eaax1396. https://doi.org/10.1126/sciadv.aax1396

Yuan, X., Wang, L., & Wood, E. F. (2018). Anthropogenic intensification of Southern African flash droughts as exemplified by the 2015/16 season. *Bulletin of the American Meteorological Society*, *99*(1), S86–S90. https://doi.org/10.1175/BAMS-D-17-0077.1

Yuan, X., Wang, L., Wu, P., Ji, P., Sheffield, J., & Zhang, M. (2019). Anthropogenic shift towards higher risk of flash drought over China. *Nature Communications*, *10*(1), 4661. https://doi.org/10.1038/s41467-019-12692-7

References From the Supporting Information

Liu, X., He, B., Guo, L., Huang, L., & Chen, D. (2020). Similarities and differences in the mechanisms causing the European summer heatwaves in 2003, 2010, and 2018. *Earth's Future*, *8*(4), e2019EF001386. https://doi.org/10.1029/2019EF001386

Shukla, P., Skeg, J., Buendia, E. C., Masson-Delmotte, V., Pörtner, H.-O., Roberts, D., et al. (2019). *Climate change and land: An IPCC special report on climate change, desertification, land degradation, sustainable land management, food security, and greenhouse gas fluxes in terrestrial ecosystems*.

Wang, D., & Tang, Y. (2014). A one-parameter Budyko model for water balance captures emergent behavior in darwinian hydrologic models. *Geophysical Research Letters*, *41*(13), 4569–4577. https://doi.org/10.1002/2014GL060509